Angewandte Chemie
Eine Zeitschrift der Gesellschaft Deutscher Chemiker

Supporting Information

© Wiley-VCH 2012

69451 Weinheim, Germany

Parallel Imaging and Template-Free Patterning of Self-Assembled Monolayers with Soft Linear Microelectrode Arrays**

*Andreas Lesch, Britta Vaske, Frank Meiners, Dmitry Momotenko, Fernando Cortés-Salazar, Hubert H. Girault, and Gunther Wittstock**

anie_201205347_sm_miscellaneous_information.pdf

Table of Contents

SI-1 Chemicals and Materials

(1-mercapto-undec-11-yl)hexa(ethylene glycol), $HS(CH_2)_{11}(OCH_2\text{-}CH_2)_6OH$ (OEG-thiol) was synthesized as described elsewhere.[1] Hexadecanethiol (HDT, Alfa Aesar, Karlsruhe, Germany), ferrocenemethanol (FcMeOH, Sigma–Aldrich, Buchs, Switzerland), $[Ru(NH_3)_6]Cl_3$ (Sigma-Aldrich, Steinheim, Germany), KBr (Sigma-Aldrich, Steinheim, Germany), KNO_3 (Sigma–Aldrich, Buchs, Switzerland, or Carl Roth, Karlsruhe, Germany) were of analytical grade and were used as received. Deionized water was produced by a Milli-Q plus 185 model (Millipore, Zug, Switzerland) or by Purelab® Classic (Elga LabWater, United Kingdom). The carbon electrodes and connection pads were fabricated by Electrador carbon ink (Electra Polymer & Chemicals Ltd., Roughway Mill, Dunk Green, England). Poly(dimethylsiloxane) (PDMS) stamps were made from Sylgard® 184 Elastomer Kit (Dow Corning, Wiesbaden, Germany).

SI-2 Preparation of Soft Linear Microelectrode Arrays

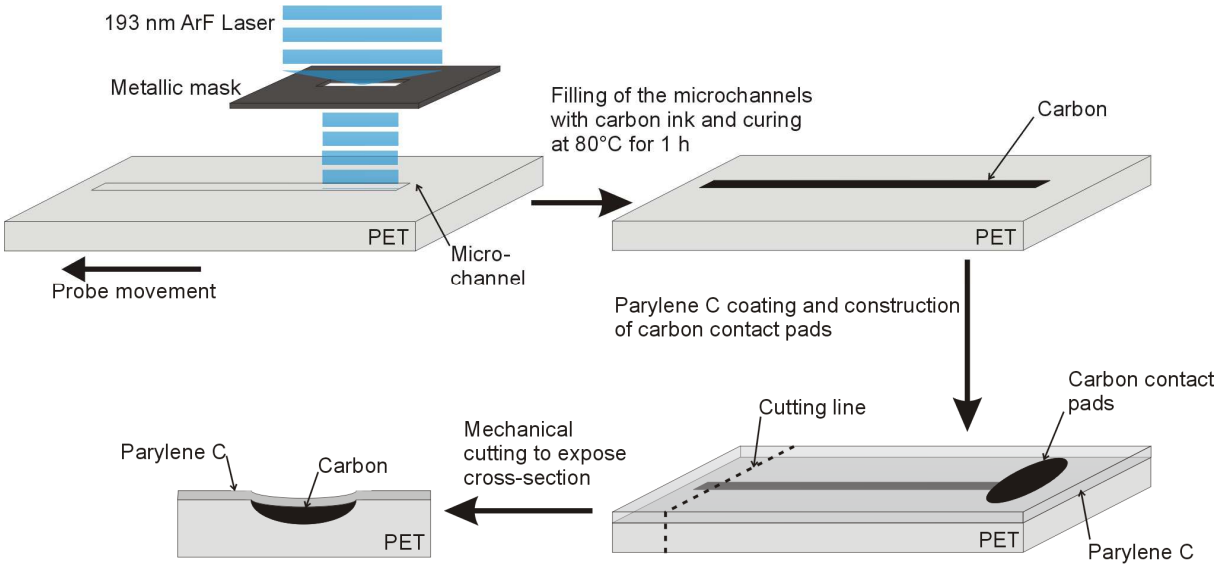

Figure SI-2.1. Schematic representation of soft probe preparation with one exemplary channel.

Soft linear microelectrode arrays consisting of eight individual electrodes were fabricated by using various successive fabrication techniques that are suitable for batch production.[2] A schematic representation is shown in Figure SI-2.1. Microchannels with 10 – 30 µm depth, 15 – 50 µm width and 7 cm length were formed by UV photoablation with a 193 nm ArF excimer laser beam (Lambda Physik, Göttingen, Germany, fluence = 0.2 J, frequency = 50 Hz). The pulsed beam was directed on a fixed metallic mask and the substrate was moved with continuous velocity in order to achieve uniform channel dimensions (*i.e.* width and depth). The channels were separated 250 µm or 500 µm (midpoint-to-midpoint distance). They were filled manually with carbon ink. After curing at 80 °C for one hour the sintered carbon tracks were covered and sealed with an insulating Parylene C layer of 3 µm thickness using a Parylene deposition system (Comelec SA, La Chaux-de-Fonds, Switzerland). Electronic connection pads for the individual electrodes were prepared by manually applying carbon ink followed by a curing process. The cross-section and therefore the active electrode areas were exposed by mechanical cutting with a razor blade mounted in a custom-made cutting device or by laser ablation. Cut arrays can be used several times for many hours. If deactivation occurred, fresh electrode surfaces were created by a new razor blade cut. In SECM experiments the Parylene C coated carbon microelectrode layer faced the sample surface providing an almost constant working distance.

SI-3 SECM Instrumentation

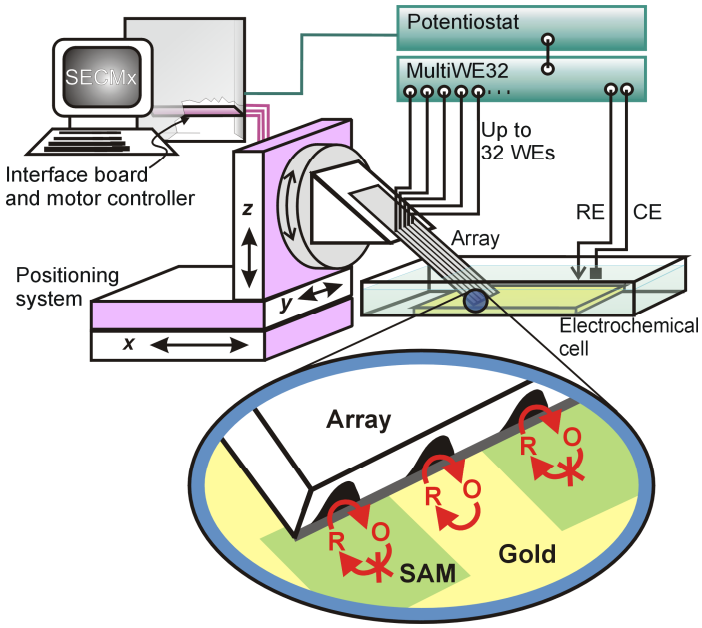

Figure SI-3.1. Schematic representation of SECM setup for high-throughput imaging and modification using soft linear microelectrode arrays.

The setup of the scanning electrochemical microscope (SECM) is shown schematically in Figure SI-3.1. Experiments were performed using a custom-built instrument consisting of a Märzhäuser three-axes positioning system (Märzhäuser Wetzlar, Wetzlar, Germany), a tilt table for mounting the electrochemical cell and for tilt elimination (Zaber Technologies, Vancouver, Canada, for clarity not shown in scheme), and an Ivium CompactStat Potentiostat (Ivium Technologies, Eindhoven, The Netherlands) connected to an Ivium MultiWE32 unit allowing the operation of up to 32 individually addressable working electrodes. The potential was controlled via one counter electrode (CE) *vs.* one reference electrode (RE). In all measurements a Pt wire served as CE and a Ag wire as quasi-RE, to which all potentials were referred. The setup can be expanded to 256 working electrodes by using eight MultiWE32 connected to one IviumStat. Online control of experiments, data acquisition and plotting was performed with the in-house made SECMx software.[2] The soft microelectrode arrays were mounted in a custom-made holder providing the electronic connection and allowing the alignment of the eight probe channels with respect to the sample by taking advantage of a worm drive (shown in the scheme as a disc). The holder was set to an inclination angle of 20° between the probe and the surface normal. Offline data handling (calibration) and plotting was performed with the in-house made software MIRA.[2].

SI-4 SECM Scanning Mode

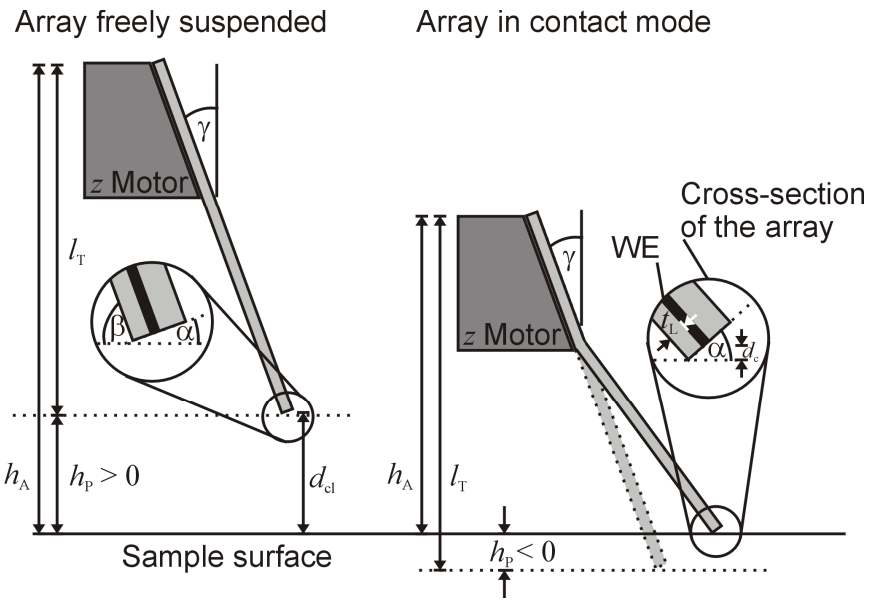

Figure SI-4.1. Schematic representation of the soft probes mounted in the custom made SECM holder for vertical approaching.

Geometric arrangement. In order to assess the influence of the bending soft probe on the working distance, some geometric considerations are provided. The array was placed in the custom made holder with an inclination angle of $\gamma = 20°$ with respect to the surface normal. It results in a vertical length l_T and a height of the attachment point above the sample h_A as shown in Figure SI-4.1, left panel. The vertical differences between these two points define the important quantity h_P.

$$h_P = h_A - l_T \qquad \text{(SI-4.1)}$$

h_P becomes negative when the probe continues approaching after mechanical contact between probe and sample. α represents the angle between the probe surface including the active electrode areas and the sample surface. Depending on the cutting angle used to expose the cross-section of the probe, α is smaller or equal γ when the array is placed in solution bulk. After mechanical contact, α increases with decreasing h_P, so that it may exceed γ. t_L represents the thickness of the thin insulating Parylene C layer and considers also the recess of the individual electrodes (Figure 1a of the main manuscript). All these quantities are required for calculation of the effective working distances in contact and contactless modes (c or cl, Equation SI-4.2 and SI-4.3).

$$\text{cl: } d_{cl} = h_P + t_L \cdot \sin(\alpha); h_P \geq 0 \qquad \text{(SI-4.2)}$$

After making contact h_P becomes negative and the working distance is calculated by

$$\text{c: } d_c = t_L \cdot \sin(\alpha); h_P < 0. \qquad \text{(SI-4.3)}$$

Vertical positioning. The vertical coordinate (z_0) for the mechanical contact between probe and the sample is found from an SECM feedback approach curve, in which the electrolysis current $i_{T,k}$ of a redox mediator, *e.g.* $[Ru(NH_3)_6]^{3+}$, is recorded at all probe electrodes (indexed by k) as function of z. An exemplary approach curve of the array probe is shown in Figure SI-4.2. The OEG SAM shows less permeability for the redox mediator. However, independently on the specific sample kinetics, $i_{T,k}$ will not change significantly when approaching further after the mechanical contact. This point defines the location of the surface. After the recording of the complete approach curve, the probe was positioned about 30 – 150 µm after z_0 (*e.g.* h_p = -40 µm) in order to make sure that the probe would stay in mechanical contact during subsequent horizontal scanning even on a slightly tilted sample. All following experiments, such as the modification or imaging with integrated automatic lift off and re-approaching steps were referred to this initially defined vertical position.

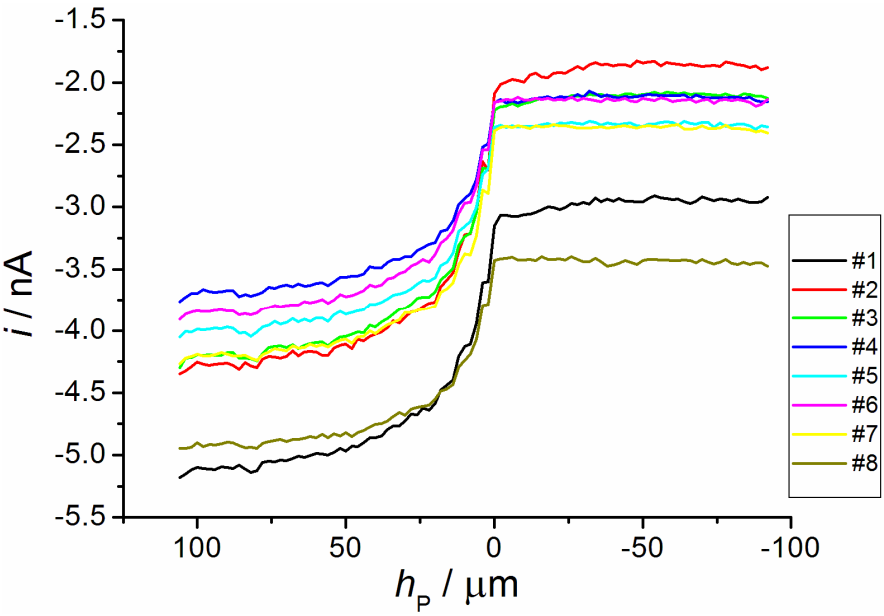

Figure SI-4.2. Approach curve with a probe array towards OEG SAM in 1 mM $[Ru(NH_3)_6]Cl_3$ and 50 mM KBr in 0.1 M phosphate buffer solution (pH = 7). Numbers indicate the number of the array elements. E_T = -0.35 V, step size 2 µm, translation rate 10 µm s^{-1}.

SECM imaging. Within SECM imaging several specific movements are performed as demonstrated schematically in Figure SI-4.3. The array starts a horizontal line scan in contact

mode ($h_P \leq 0$ µm) in the so-called “high frequency” (HF) direction. The term HF refers to the situation that in this direction values are recorded with a much higher frequency than in the perpendicular horizontal direction. The latter one is named “low frequency” (LF) axis. Usually the HF direction is set to the *x* and the LF direction to the *y* axis. The HF direction must be in the direction of the probe inclination. After reaching the full distance of the first HF line scan, the soft probe is lifted off the sample (LO) by a defined stroke height so that it is freely suspended in solution bulk. Then the probe is moved back the HF scan length to the horizontal starting position with high translation rates (up to 1000 µm s^{-1}) without current recording, followed by a step in the LF direction, and a re-approach by the stroke height in order to reach again the h_P value for which the first line scan was recorded. Afterwards the next line scan with current recording is started. During the experiment, the individual electrodes will eventually scan over an area that was already scanned by the adjacent electrode. For this purpose a multiple imaging routine was implemented in which the array (lifted off the sample) performs a large step in the LF direction (red line in Figure SI-4.3) and is placed besides the last scan of the *k*-th electrode, *i.e.* on previously not investigated regions. The next line scan is started there. In this way several adjacent image frames can be scanned in just one experiment providing a data set that can be processed as one experiment offline in MIRA to construct one complete image.

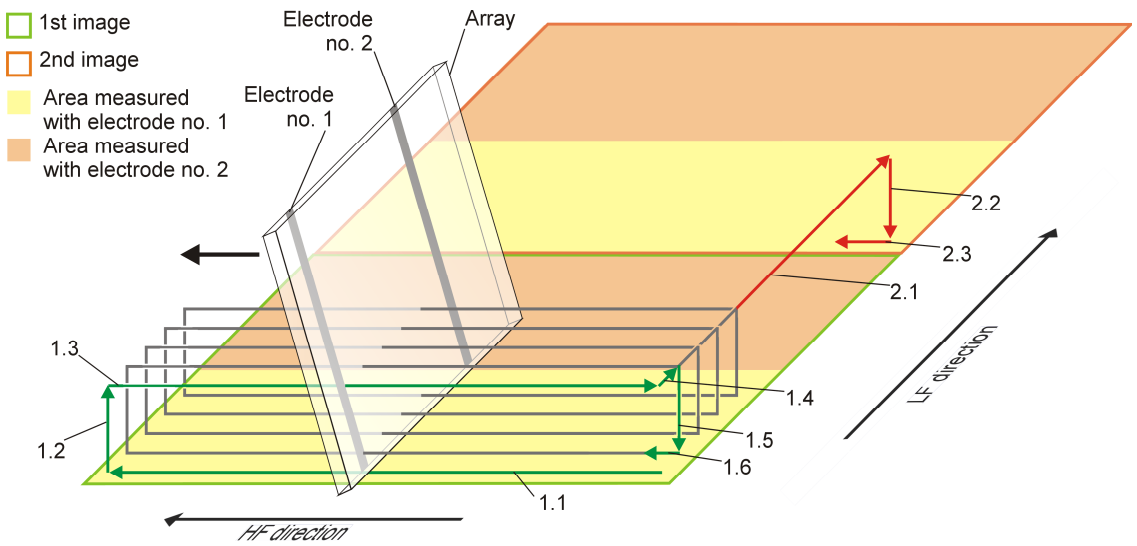

Figure SI-4.3. Schematic representation of multiple SECM imaging. Movement of one soft array with two electrodes (two electrodes were chosen for clarity; experiments were performed with arrays of up to eight microelectrodes). 1 – first image: 1.1 – first HF fwd line scan (recording), 1.2 – lift-off, 1.3 – first HF rev scan (no recording), 1.4 – LF fwd step, 1.5 – re-approach, 1.6 – start of second HF fwd scan; 2 – second image: 2.1 – large step, 2.2 – re-approach, 2.3 – start of first HF fwd line scan.

SI-5 SECM Imaging of SAM Patterns by µCP - Calibration of Signals from Individual Array Elements

Preparation of gold surfaces and SAM. Gold substrates were freshly prepared on cleaned microscope slides by vapor deposition of chromium (0.5 nm) and then gold (100 nm). The stamp had squares of 50 µm × 50 µm and a periodicity of 70 µm in both directions. For µCP a PDMS stamp was casted from a silicon master obtained by photolithography. It had elevated squares of 50 µm × 50 µm and a periodicity of 70 µm (20 µm space between squares). The stamp was inked in a 1 mM ethanolic solution of HDT and dried afterwards for 2 min under a stream of nitrogen. The stamp covered with HDT was then pressed gently for 1 min on the Au surface. The Au surface was rinsed with pure ethanol after removal of the stamp followed by drying under a stream of nitrogen. In order to form a homogenous monolayer, the Au samples were immersed for 12 h in a 3 mM ethanolic solution of self synthesized OEG-terminated thiol ($HS(CH_2)_{11}(OCH_2CH_2)_6OH$) followed by rinsing with pure ethanol and drying under a stream of nitrogen. In all experiments the samples were unbiased.

SECM imaging parameters: Reactivity imaging in SECM feedback mode of µCP SAM was performed in 2 mM FcMeOH and 0.1 M KNO_3 with a probe potential of E_T = 0.4 V. Following general custom, all applied potentials and measured currents are indexed with "T" (for "tip") being aware that the array electrodes are flat sickle-shaped areas. (Other imaging parameters are given in the SI at the places were details for the corresponding samples are collected).

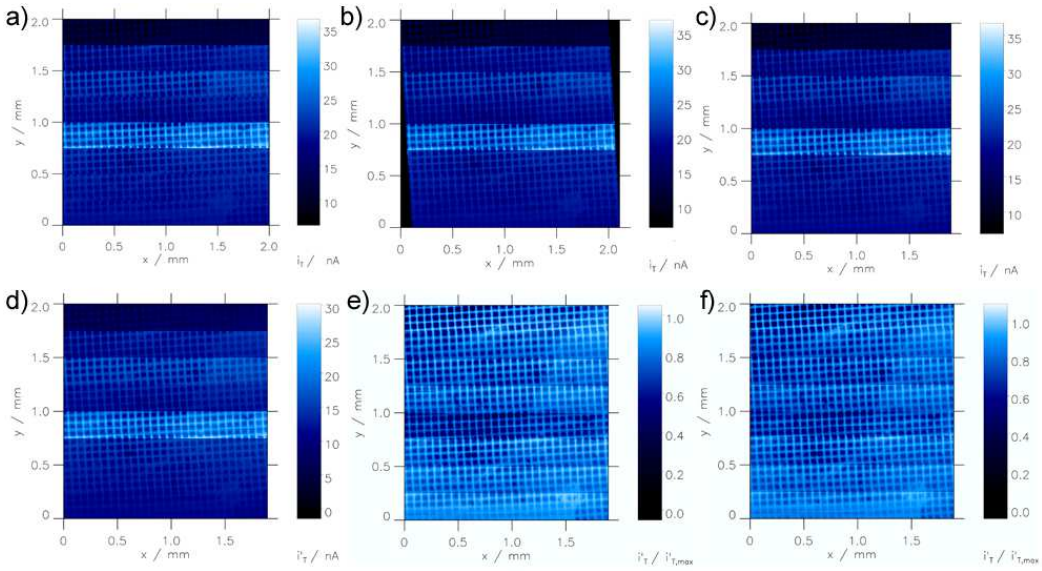

Figure SI-5.1. Calibration of measured currents. a) Original currents and original x values. b) Corrected $x_{\mathrm{offs},k}$. c) Subsets were cut in order to eliminate protruding areas without measured values. d) Image after applying $i_{\mathrm{T,offs},k}$ from approach curves. e) Image after application of s_k. f) Final image after minor manual corrections of the calibration.

Experimental condition used for Figure 2b: h_{P} = -46 µm, LO stroke height 300 µm, LO retract speed 250 µm s^{-1}, LO approach speed 10 µm s^{-1}, HF fwd step size 5 µm, HF fwd translation rate 25 µm s^{-1}, HF fwd delay before data acquisition 0.1 s, HF rev translation rate 250 µm s^{-1}, LF fwd step size 5 µm, LF fwd translation rate 25 µm s^{-1}, total imaging time 5.5 h. The original currents of the eight sensors vary slightly due to small differences in geometry, size and working distance. In addition, electrodes have small variations in their recess depth. These effects are caused by the fabrication and cutting processes. The currents can be calibrated offline using the software tool MIRA. Positional offsets exist and can be corrected as well. The positional offsets between the individual electrodes k in LF direction (called $y_{\mathrm{offs},k}$) are well defined by the laser fabrication process. Therefore, each y position on an individual electrode y_k is corrected to give y'_k. All correction values of the investigated SAM grid in Figure 2b of the main manuscript are listed in Table SI-5.1.

$$y'_k = y_k + y_{\mathrm{offs},k} \qquad \text{(SI-5.1)}$$

The original currents and x positions of Figure 2b of the main manuscript are plotted without corrections in Figure SI-5.1a that considers the positional offsets in y direction. Positional offsets along the HF direction $x_{\mathrm{offs},k}$ are caused by the manual cutting procedure or a misalignment due to the placement in the holder. They are corrected similar to the y positions

(Figure SI-5.1b). They can be determined from well-defined surface structures, *e.g.* a sharp line perpendicular to the scan direction or by imaging rectangular shapes.

$$x'_k = x_k + x_{\mathrm{offs},k} \tag{SI-5.2}$$

The correction will restore right angles in the image of rectangular sample features (Figure SI-5.1b). The edges of the image are clipped to yield again to a rectangular image frame (Figure SI-5.1c). The currents of an individual electrode remain constant when the array is in contact with the sample of uniform reactivity ($h_P < 0$ µm), but vary between different electrodes. This is clearly observed in Figure SI-5.1a-c. Therefore, a calibration routine was developed in order to level the current responses between individual electrodes in one array. An electrode-depended current offset $i_{T,\mathrm{offs},k}$ (*i.e.* the measured current above a plane region over which the minimum absolute currents $i_{T,\mathrm{min},k}$ result) is subtracted from the original currents $i_{T,k}$ of each electrode.

$$i'_{T,k} = i_{T,k} - i_{T,\mathrm{offs},k} \tag{SI-5.3}$$

These current offsets can be interpreted in various ways. It corrects for instrumental limitations of the device as well as current variations due to slightly different effective working distances.

$$i_{T,\mathrm{offs},k} = i_{T,\mathrm{min},k} \tag{SI-5.4}$$

We want to stress that soft probes have been developed for imaging. They are so far not for extracting quantitative kinetic information due to geometric variations. For the measurement in Figure SI-5 $i_{T,\mathrm{min},k}$ is the negative feedback current which can be derived from approach curve measurements on an insulating substrate (here glass, not shown). Alternatively, these current values can also be extracted from line scans. The procedure using Equation SI-5.3 sets the current for negative feedback to 0.0 (Figure SI-5.1d). An electrode depended scale factor s_k was used to compensate for size and distance variations in positive feedback experiments. s_k is now applied to set the maximum corrected currents of each individual electrode to 1.0. For this purpose s_k is the reciprocal of the offset-corrected maximum current $i'_{T,\mathrm{max},k}$ (Equation SI-5.5).

$$s_k = \frac{1}{i'_{T,\mathrm{max},k}} = \frac{1}{i_{T,\mathrm{max},k} - i_{T,\mathrm{offs},k}} \tag{SI-5.5}$$

The relative currents are then calculated by Equation SI-5.6. This procedure is done for all SECM images in contact regime.

$$\frac{i'_{T,k}}{i'_{T,\mathrm{max},k}} = \left(i_{T,k} - i_{T,\mathrm{offs},k}\right) \cdot s_k \tag{SI-5.6}$$

The image after these corrections is shown in Figure SI-5.1e. Despite those corrections other sources of variation do exist. The soft probes can change during the experiment in a different way which makes manual correction of $i_{T,offs,k}$ necessary done for the fourth sensor (Table SI-5.1). Figure SI-5.1f shows the result after all performed corrections. This is the image reproduced as Figure 2b of the main manuscript.

Table SI-5.1. Positional offsets, current offsets and scale factors of the individual electrodes determined by approach curve analysis used for Figure 2b.

Electrode no. k	$x_{offs,k}$ (µm)	$y_{offs,k}$ (µm)	$i_{T,offs,k}$ (nA)[a]	s_k (nA^{-1})
1	0	0	7.78	0.076
2	15	250	7.15	0.066
3	30	500	6.43	0.057
4	45	750	6.23 (4.50)	0.034
5	60	1000	6.57	0.064
6	75	1250	6.13	0.050
7	90	1500	6.76	0.062
8	110	1750	4.76	0.111

[a] The value in brackets represents a manually adjusted current offset used for Figures 2b and SI-5.1f

Figure 2c of the main manuscript shows a corrected image of Figure SI-5.2a. The image was recorded using the multiple SECM imaging mode with one large step, thus the image is constructed from two adjacent image frames. The correction was performed by approach curve analysis with the values shown in Table SI-5.2. No manual adjustment was required. Figure SI-5.2b shows the same image after correction and is reproduced as Figure 2c (main manuscript). The image was recorded using the following parameters.

Experimental condition used for Figure 2c: h_P = -46 µm, LO stroke height 300 µm, LO retract speed 250 µm s^{-1}, LO approach speed 10 µm s^{-1}, HF fwd step size 10 µm, HF fwd translation rate 25 µm s^{-1}, HF fwd delay before data acquisition 0.1 s, HF rev translation rate 250 µm s^{-1}, LF fwd step size 10 µm, LF fwd translation rate 25 µm s^{-1}, LF large step size 2000 µm total imaging time 7 h.

Table SI-5.2. Positional offsets, current offsets and scale factors of the individual electrodes determined by line scan analysis used for Figure 2c.

Electrode no. k	$x_{offs,k}$ (µm)	$y_{offs,k}$ (µm)	$i_{T,offs,k}$ (nA)	s_k (nA^{-1})
1	0	0	9.83	0.075
2	-4.5	250	8.93	0.065
3	-9	500	8.11	0.055
4	-13.5	750	7.71	0.036
5	-18	1000	8.03	0.061
6	-22.5	1250	7.43	0.048
7	-27.0	1500	8.03	0.058
8	-31.5	1750	4.98	0.110

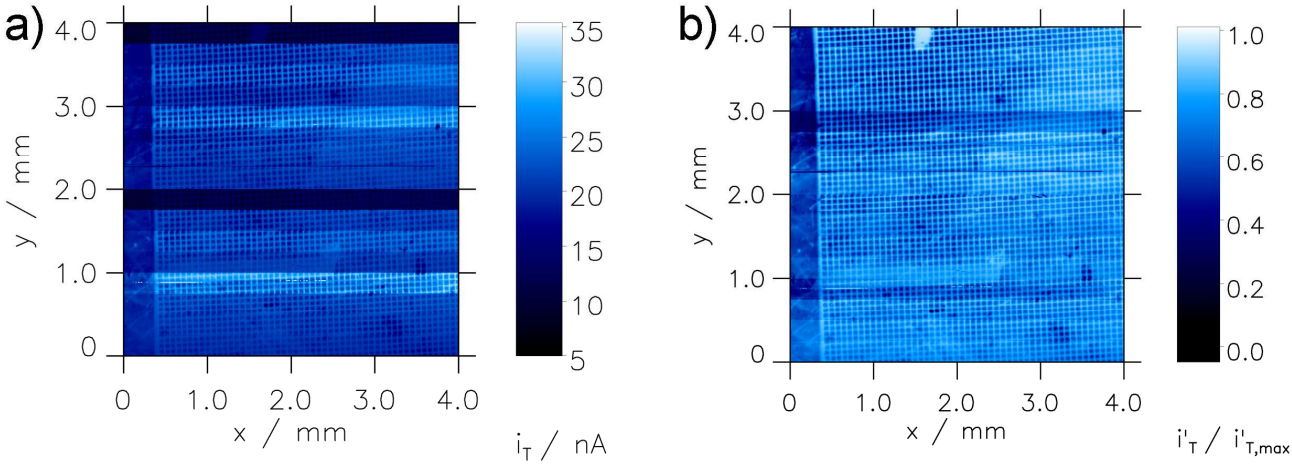

Figure SI-5.2. Original currents (a) and calibrated currents (b) of Figure 2c in the main manuscript using correction values of Table SI-5.2.

The sensitivity of the µCP SAM was demonstrated by scratching the structure gently with a polymeric Eppendorf pipette tip. Afterwards SECM imaging was performed with an array of eight microelectrodes (Figure SI-5.3). The removed parts of the SAM can be identified clearly. This result highlights the possibility of scanning delicate patterns like SAMs with our soft probes without damaging the sample or the probe itself. The fourth sensor got broken while scanning. Therefore, the stripes in the middle of the image are caused by the measurement and not by the substrate. This can happen after long term usage. The probe was used without a

refreshing by a new blade cut for Figures SI-5.1-3. However, the other seven sensors did not show abuse.

Experimental condition used for Figure SI-5.3: h_P = -46 µm, LO stroke height 300 µm, LO retract speed 250 µm s^{-1}, LO approach speed 10 µm s^{-1}, HF fwd step size 10 µm, HF fwd translation rate 25 µm s^{-1}, HF fwd delay before data acquisition 0.1 s, HF rev translation rate 250 µm s^{-1}, LF fwd step size 10 µm, LF fwd translation rate 25 µm s^{-1}, total imaging time 2 h.

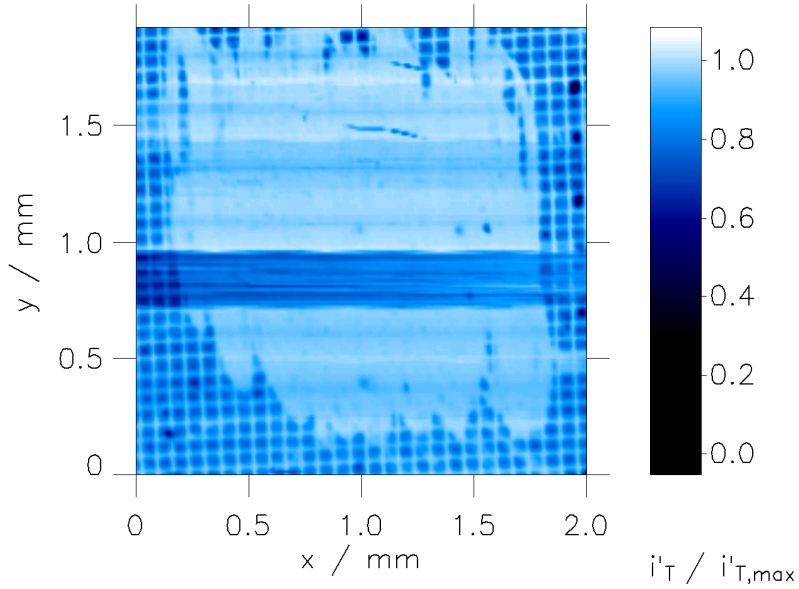

Figure SI-5.3. Calibrated image of the µCP SAM structure after gentle scratching with a plastic Eppendorf pipette tip.

SI-6 Shape of the Modified Regions

SECM: Modification of the OEG SAM was performed with a soft carbon microelectrode in contact mode. The electrode rested in 1 mM $[Ru(NH_3)_6]Cl_3$ and 50 mM KBr in 0.1 M phosphate buffer solution (pH = 7) and a 5 seconds pulse to E_T = +1.8 V was applied to generate Br_2/HOBr. A conventional Pt UME enclosed in a glass sheath (tip radius r_T = 12.5 µm) was used in the same electrolyte and positioned with a working distance d = 3 µm above the modified region and SECM reactivity imaging was performed by recording the reduction current of $[Ru(NH_3)_6]^{3+}$ at E_T = -0.35 V (Figure 3a of the main manuscript).

Experimental condition used for Figure 3a: HF fwd and rev step size 2 µm, HF fwd and rev translation rate 25 µm s^{-1}, HF fwd and rev delay before data acquisition 0.1 s, LF fwd step size 2 µm, LF fwd translation rate 25 µm s^{-1}.

CLSM: For selective adsorption of extracellular matrix proteins, the modified sample was immersed for 4 h in 100 µg mL^{-1} fibrinogen-Alexa 488 in phosphate buffered saline (0.1 M phosphate, 0.15 M NaCl, pH = 7.4). With a confocal laser scanning microscope (TCS SP2 AOBS, Leica Microsystems GmbH, Wetzlar, Germany) the dye was excited at a wavelength of 488 nm and the fluorescence was detected with a spectral range of 500-535 nm.

PFM SFM: Pulsed force mode (PFM) scanning force microscopy (SFM) was performed under ambient conditions with a Nanoscope IIIA controller, a Dimension 3100 sample stage and a Dimension "G" scanning head (all Veeco Instruments Inc., Santa Barbara, CA, USA) operating in pulse force mode (WITec, Ulm, Germany).[3, 4] Topography, stiffness, and adhesion were recorded. The Au-coated SFM tip (Olympus OMCL-RC800PB, 0.82 N/m) was modified in 1 mM 11-mercaptoundecanoic acid to form a COOH-terminated SAM as described previously in order to detect the hydrophilic and hydrophobic parts of the monolayer.[5] A 256 × 256 pixel image of a 100 µm × 100 µm area was recorded with a scan rate of 0.5 Hz. Image flattening was performed by subtracting a background from the raw data in order to eliminate the vertical offset between line scans and the tilt in each line scan. The background was found by finding as a least-squares fit to first-order (for adhesion and stiffness) and third-order (for topography) polynomials for the selected image region using the Nanoscope software (V5.30r3sr3).

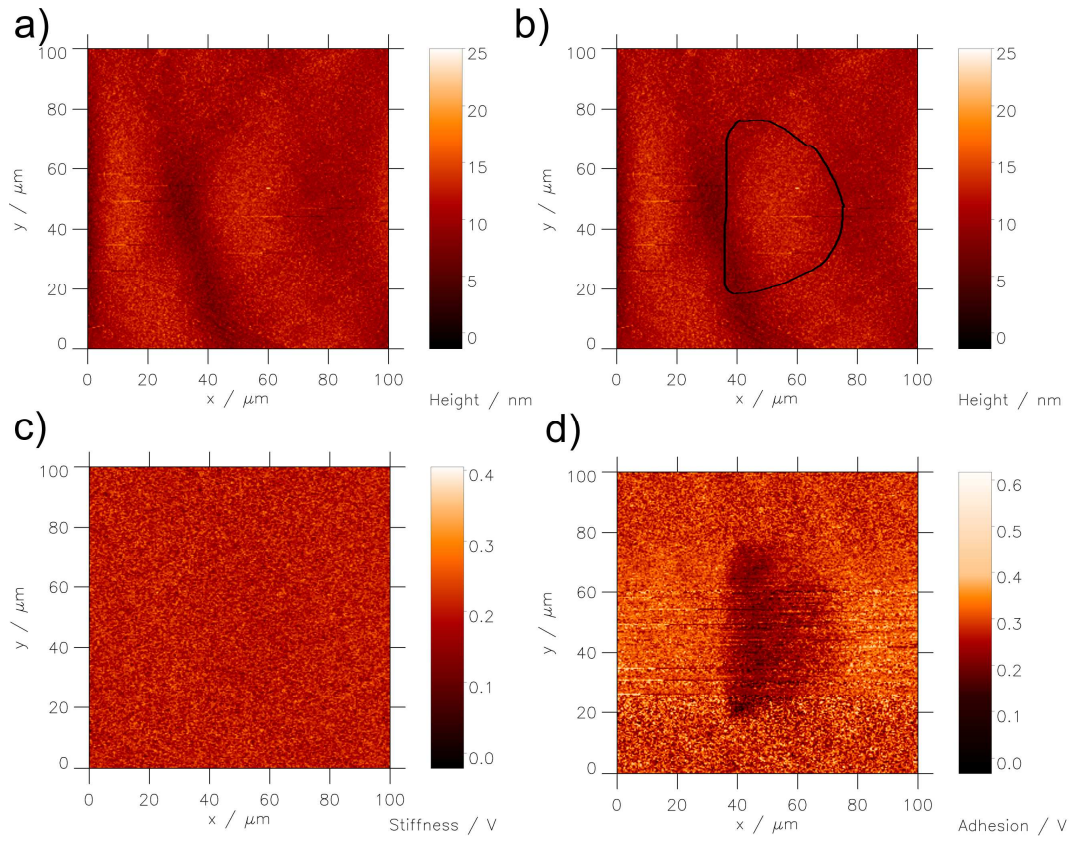

Figure SI-6.1. PFM SFM images of the modified OEG SAM. a) Topography, b) Topography with overlaid etched area from the adhesion image (d), c) Stiffness, d) Adhesion.

PFM SFM is a non-resonant, intermediate-contact technique that gives information about surface properties such as topography, stiffness, and adhesion. These surface characteristics of one modified spot were recorded in one measurement and are plotted in Figure SI-6.1. No significant changes in the topographic image SI-6.1a are found because the thickness of the monolayer is much smaller than the roughness of the used gold substrates. A clear contrast is detected only for adhesion (Figure SI-6.1d). The outline of the etched area in the adhesion image was overlaid with topographic image and demonstrates the independence of the topographic features from the probe-induced surface modification (Figure SI-6.1b). The horizontal stripes, in particular in the adhesion image, are caused by the measurement and do not represent real surface features. The adhesion relies on the interaction of the hydrophilic tip with the hydrophilic (OEG-terminated SAM) and hydrophobic (chemically modified OEG SAM) parts of the sample surface and are enhanced by the natural condensed water film on the sample at ambience conditions. The shape of the non-adhesive (the modified) region fits to the SECM feedback image (Figure 3a of the main manuscript). Since the SECM image relies on the diffusion of a redox mediator and because a much bigger disk was used for image recording compared to the SFM tips, PFM SFM gives a much more precise image of

the real dimension of the modified spot. The shape of the modified spot appears much sharper on the left side. This is due to the much more defined diffusion of Br_2/HOBr during the modification in this region. The Parylene C coating was in contact with the sample and restricted the diffusion of Br_2/HOBr on this side leading to a sharp transition between modified and unmodified regions. To the right the working distance increased and the Br_2/HOBr diffusion was less efficient. This can be seen in two effects in Figure SI-6.1d: i) the measured signal within the modified spot increased from left to right demonstrating slightly hydrophilic properties caused probably by some residual OEG units and ii) the border between the modified and unmodified OEG SAM at the right is less sharp than the border at the left.

SI-7 High-Throughput Surface Modification and Imaging

SECM modification and imaging: One solution was used for the microelectrochemical modification *and* SECM feedback mode imaging consisting of 1 mM $[Ru(NH_3)_6]Cl_3$ and 50 mM KBr in 0.1 M phosphate buffer solution (pH = 7). A base potential was applied to all electrodes from the Ivium potentiostat and MultiWE32 unit. Individual offset potentials in the range of ± 2 V with respect to the base potential can be applied to individual electrodes. We took advantage of this by inducing the Br_2/HOBr generation at potentials $E_{T,on}$ = +1.9 V while a significantly lower base potential $E_{T,off}$ = +0.1 V applied over regions that should not be modified. During pulsing the array was not moved. The steps between the modifications were 100 µm. The array (midpoint-to-midpoint distance 500 µm) was moved with 25 µm s^{-1} and a delay of 0.5 s was set before the modification. The total time for the line scan was 58 s. By applying a potential of E_T = -0.35 V the steady state reduction of $[Ru(NH_3)_6]^{3+}$ was used for feedback mode imaging.

Experimental condition used for Figure 4b: h_P = -140 µm, LO stroke height 200 µm, LO retract speed 100 µm s^{-1}, LO approach speed 10 µm s^{-1}, HF fwd step size 10 µm, HF fwd translation rate 25 µm s^{-1}, HF fwd delay before data acquisition 0.1 s, HF rev translation rate 1000 µm s^{1}, LF fwd step size 10 µm, LF fwd translation rate 25 µm s^{-1}, total time required was 26 min.

The calibration procedure from SI-5 was also used for Figure 4b and c. The calibration values and the original and corrected images are shown in Table SI-7.1 and Figure SI-7.1, respectively. Calibration values were derived from line scan experiments. $i_{T,min,k}$ and $i_{T,max,k}$ are the current values measured over non-permeable and modified OEG SAM, respectively.

Table SI-7.1. Current offsets and scale factors of the individual electrodes determined by line scans.

Electrode no. k	$i_{T,offs,k}$ (nA)	s_k (nA^{-1})
1	-4.27	-0.20
2	-3.44	-0.13
3	-3.37	-0.10
4	-4.00	-0.22
5	-3.78	-0.36
6	-3.96	-0.23
7	-3.03	-0.12
8	-3.39	-0.05

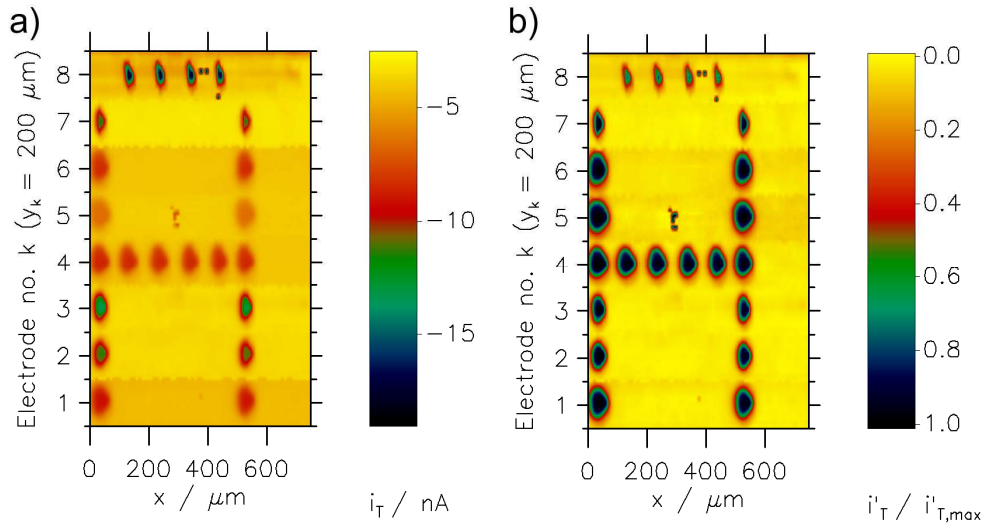

Figure SI-7.1. Original currents (a) and calibrated currents (b) of modified “A” pattern using correction values of Table SI-7.2.

SI-8 From jpg-File to SECM High-Throughput Surface Modification

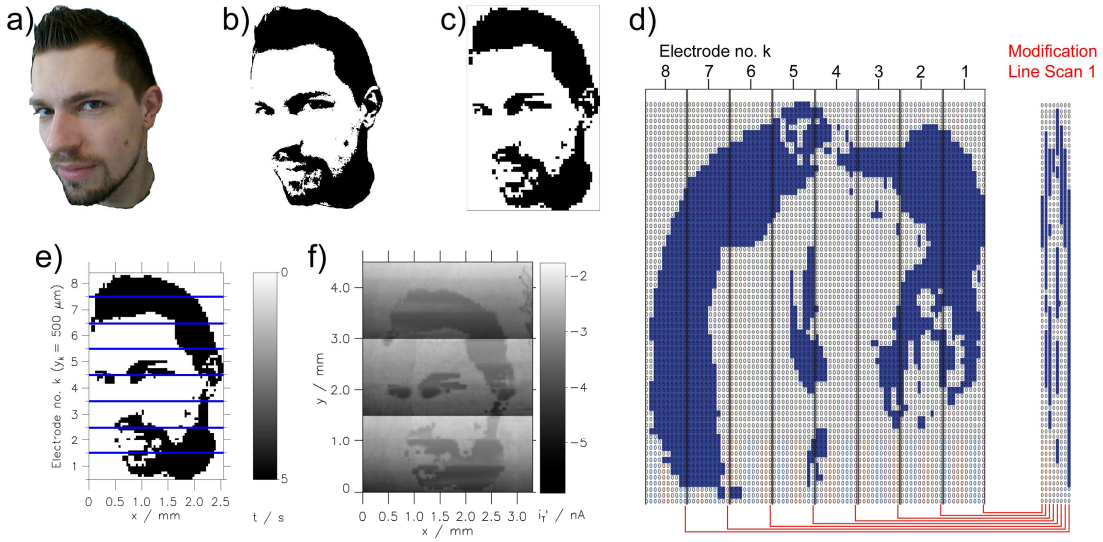

Figure SI-8.1. Representation of the performance from a photograph to an SECM image. a) Photograph taken with a digital camera (2560 × 1920 pixels). b) Converted black-white two color scale (2560 × 1920 pixels). c) Black white tiff file with 80 × 69 pixels, pixel ratio *x*/*y* = 0.75. d) Left: Into pulse lengths (0 s, not highlighted; 5 s, highlighted in blue) converted ASCII file. Ten line scans per electrode can be extracted for ten line scan modification files for SECMx as shown exemplary for the first line scan (right). e) Plotted pulse seconds after performed modification. The individual areas from the individual sensors are marked. f) SECM feedback image.

In the following section the complete succession from a graphic file (jpg) to the transfer into a SAM layer and SECM feedback imaging is detailed. An optical photograph was taken with a digital camera of a mobile phone (2560 × 1920 pixels, Samsung Galaxy S I9000, Samsung Electronics, Republic of Korea) and saved in jpg-format. This file was loaded in Adobe Photoshop CS2 (Version 9.0). First the background was cut (Figure SI-8.1a). Then the picture was converted into a black-white two color scale (Figure SI-8.1b). For SECM high-throughput modification a compromise was made between resolution and image size. Finding appropriate parameters with respect to step sizes and spot shape was crucial for the experimental performance. The sizes of the sickle-shaped modified spots are given by the electrode geometries, working distances and the amount of Br_2/HOBr reaching the OEG SAM. Therefore, an average spot size can be assumed from the PFM SFM image (SI-6) of 60 µm (*y* direction) and 40 µm (*x* direction). In order to get overlapping modified regions (*i.e.* continuous modified regions) the spot distance was set to 50 µm value (*y*) and 37.5 µm (*x*). With these settings the image can be represented by 80 × 69 pixels (LF (*y*) × HF (*x*), Figure SI-8.1c, saved as TIFF).

Such an image can be realized if the 8 individual electrodes of an array with 500 µm electrode separation perform 10 line scans (8 × 10 *y* positions) in *x* direction with 69 steps. This will transfer the image on an area of 3950 µm × 2550 µm.

The software tool “ascii-pixelhaufen” was used to transfer the two level TIFF file into a two character text file in ASCII format (ascii-pixelhaufen 2008.exe, Ruben Demus). The "table" representing the file content is shown in Figure SI-8.1d (left). Cells of the table that encode surface modifications are coloured blue. Due to the order of electrodes within the array the first ten columns from right to left refer to the 1st sensor, the next ten to the 2nd and so on. Ten modification line scan files were extracted from the table and arranged to a line scan modification file as input data for SECMx, *e.g.* like Figure SI-8.1d (right). In this way the 8 electrodes modified the areas that are separated by blue lines in Figure SI-8.1e. The “off” potential (no modification) of $E_{T,off}$ = 0.1 V, and the “on” potential $E_{T,on}$ = 1.5 V to generate Br_2/HOBr for modification were set together with the step sizes of 37.5 µm and a delay of 0.5 s before and after applying a pulse. The array electrode itself was moved in contact mode on the surface with a translation rate of 100 µm s^{-1} between modification pulses.

After completing the 10 modification line scans, SECM imaging was carried out for the modified region in the same solution by switching the potential to the diffusion limited reduction of the $[Ru(NH_3)_6]^{3+}$ at E_T = -0.3 V (Figure SI-8.1f). The time required for 10 line scans was 87 min.

Experimental condition used for Figure 5b: h_P = -40 µm, LO stroke height 500 µm, LO retract speed 100 µm s^{-1}, LO approach speed 20 µm s^{-1}, HF fwd step size 10 µm, HF fwd translation rate 100 µm s^{-1}, HF rev translation rate 1000 µm s^{-1}, LF fwd step size 12.5 µm, LF fwd translation rate 50 µm s^{-1}. Three electrodes that were separated by 1500 µm were used to cover an area of 3300 µm × 4487.5 µm. The image is composed of 119,160 individual data points (3 electrodes recorded 120 line scans each having 331 steps within one line scan) acquired within 6.5 h. A current calibration was applied with current offsets to give i'_T. A scale factor was *not* required.

For obtaining another proof of the surface modification, the sample was cooled down using a Peltier element in order to cause water condensation in the hydrophilic parts of the sample (Figure SI-8.2, right). Hydrophilic non-modified and hydrophobic modified regions can be clearly identified. It is also evident that some line scans lead to less effective surface modifications that are in a less clear way also identified at the same location in the SECM image. The eight areas modified by different electrodes can be clearly distinguished because the contrast of modification increased from line scan to line scan likely because of an

activation of the carbon electrodes by the reactive bromine species. As a result more bromine could be produced at identical pulse conditions.

Figure SI-8.2. Comparison of the modified OEG SAM by SECM (a) and by optical photography (b).

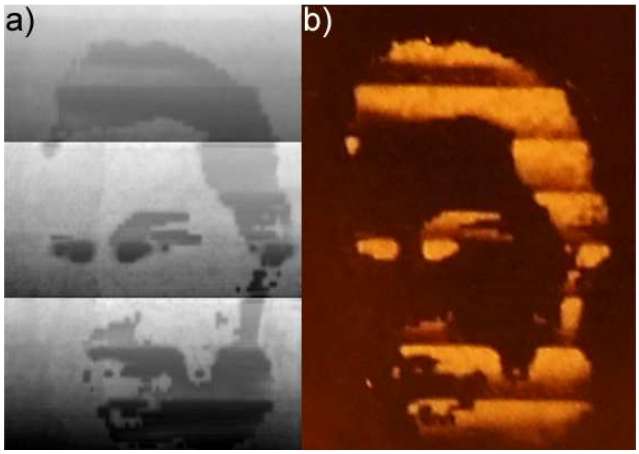

References

[1] R. Jogireddy, I. Zawisza, G. Wittstock, J. Christoffers, *Synlett* **2008**, 1219.

[2] F. Cortes-Salazar, D. Momotenko, A. Lesch, G. Wittstock, H. H. Girault, *Anal. Chem.* **2010**, *82*, 10037.

[3] Y. Okabe, U. Akiba, M. Fujihira, *Appl. Surf. Sci.* **2000**, *157*, 398.

[4] T. Miyatani, M. Horii, A. Rosa, M. Fujihira, O. Marti, *Appl. Phys. Lett.* **1997**, *71*, 2632.

[5] C. Zhao, M. Burchardt, T. Brinkhoff, C. Beardsley, M. Simon, G. Wittstock, *Langmuir* **2010**, *26*, 8641.